Supporting Information

Photomodulation of Vesicle Dynamics Using Fluorescent Photoswitchable Amphiphiles

Paola Albanese[†a,d], Simone Cataldini[†a], Simona Amoroso[a], Lucia Sessa[b], Stefano Piotto[b], Miriam Di Martino[b], Simona Concilio[b], Ilektra Mavromatidou[a], Mohinder M. Naiya[e,f], Jlenia Brunetti[c], Emiliano Altamura[g], Agnese Magnani[a], Jack L.-Y. Chen[a,e,f], Federico Rossi[d]*.*

[a] Department of Biotechnology, Chemistry and Pharmacy, University of Siena, Italy

[b] Department of Pharmacy, University of Salerno, Italy

[c] MedBiotech Hub and Competence Center, Department of Medical Biotechnologies, University of Siena, Italy

[d] Department of Physical Sciences, Earth and Environment, University of Siena, Italy

[e] School of Science, Auckland University of Technology, Auckland 1142, New Zealand

[f] The MacDiarmid Institute for Advanced Materials and Nanotechnology, Wellington, New Zealand

[g] Department of Chemistry, University of Bari "Aldo Moro", Italy

* FR: federico.rossi2@unisi.it; JLYC: jack.chen@unisi.it;

[†] These authors contributed equally

1. Characterization data for synthesized compounds

(*E*)-2-(3-(4-((4-(Octyloxy)phenyl)diazenyl)phenoxy)propyl)isoindoline-1,3-dione (6)

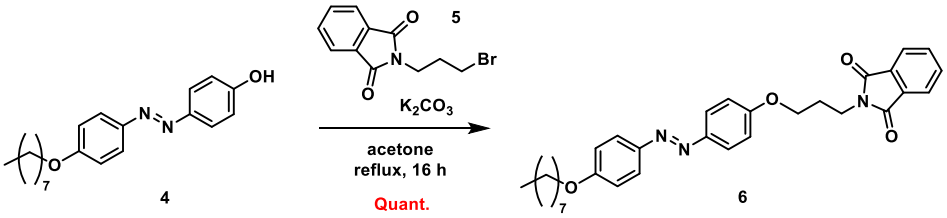

^{1}H NMR (400 MHz, $CDCl_3$): δ 7.87 – 7.79 (m, 6H), 7.73 – 7.68 (m, 2H), 6.99 – 6.94 (m, 2H), 6.89 – 6.84 (m, 2H), 4.09 (t, *J* = 6.0 Hz, 2H), 4.01 (t, *J* = 6.6 Hz, 2H), 3.92 (t, *J* = 6.8 Hz, 2H), 2.21 (qui, *J* = 6.4 Hz, 2H), 1.83 – 1.75 (qui, 2H), 1.50 – 1.40 (qui, 2H), 1.39 – 1.24 (m, 8H), 0.87 (t, *J* = 6.9 Hz, 3H). **^{13}C NMR** (101 MHz, $CDCl_3$): δ 168.4, 161.2, 160.6, 147.1, 146.9, 133.9, 132.1, 124.3, 124.2, 123.3, 114.6, 68.3, 66.0, 35.4, 31.8, 29.3, 29.2, 28.2, 26.0, 22.6, 14.1. **IR** (neat) *ν* 2923, 2868, 1768, 1707, 1594, 1499, 1393, 1240, 1068, 840, 720 cm^{-1}. The spectroscopic data is in agreement with literature values [1].

(*E*)-3-(4-((4-(Octyloxy)phenyl)diazenyl)phenoxy)propan-1-amine (7)

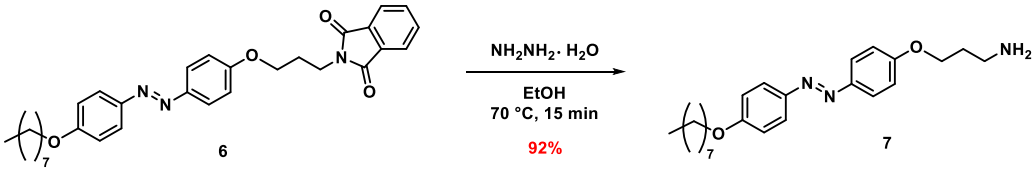

^{1}H NMR (400 MHz, $CDCl_3$): δ 7.84 (d, *J* = 8.4 Hz, 4H), 7.02 – 6.91 (m, 4H), 4.10 (t, *J* = 6.0 Hz, 2H), 4.00 (t, *J* = 6.4 Hz, 2H), 2.91 (t, *J* = 6.8 Hz, 2H), 1.93 (p, *J* = 6.5 Hz, 2H), 1.84 – 1.73 (m, 2H), 1.44 (dd, *J* = 15.0, 7.1 Hz, 2H), 1.39 – 1.22 (m, 8H), 0.87 (t, *J* = 6.7 Hz, 3H). **^{13}C NMR** (101 MHz, $CDCl_3$): δ 161.2, 160.9, 147.0, 146.9, 124.3, 114.6, 68.3, 66.1, 39.1, 33.0, 31.8, 29.3, 29.2, 26.0, 22.6, 14.1. **HRMS** calcd for $C_{23}H_{34}N_3O_2$ $[M+H]^+$ 384.26455, found 384.2644. **IR** (neat) ν 3317, 2920, 2851, 1600, 1579, 1495, 1472, 1239, 841 cm^{-1}

(*E*)-7-(Diethylamino)-*N*-(3-(4-((4-(octyloxy)phenyl)diazenyl)phenoxy)propyl)-2-oxo-2*H*-chromene-3-carboxamide (S1)

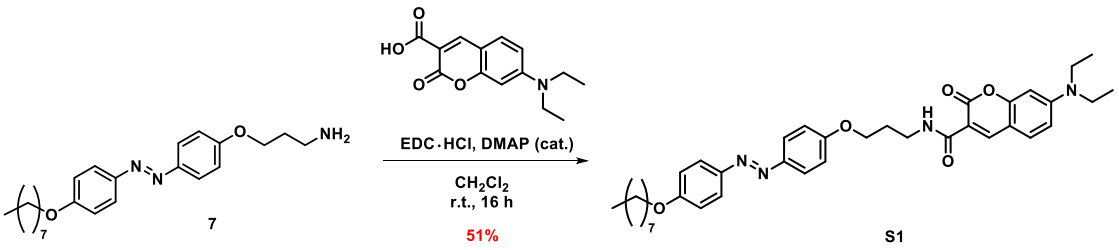

^{1}H NMR (400 MHz, $CDCl_3$): δ 9.01 (t, *J* = 5.6 Hz, 1H), 8.68 (s, 1H), 7.88 – 7.79 (m, 4H), 7.44 – 7.37 (d, 1H), 7.06 – 6.99 (m, 2H), 6.99 – 6.92 (m, 2H), 6.62 (dd, *J* = 9.0, 2.5 Hz, 1H), 6.48 (d, *J* = 2.3 Hz, 1H), 4.13 (t, *J* = 6.0 Hz, 2H), 4.00 (t, *J* = 6.6 Hz, 2H), 3.65 (q, *J* = 6.5 Hz, 2H), 3.46 – 3.39 (q, 4H), 2.14 (p, *J* = 6.3 Hz, 2H), 1.86 – 1.71 (p, 2H), 1.50 – 1.40 (p, 2H), 1.32 (m, *J* = 15.4, 10.4, 2.8 Hz, 8H), 1.21 (t, *J* = 7.2 Hz, 8H), 0.90 – 0.83 (t, 3H). **^{13}C NMR** (101 MHz, $CDCl_3$): δ 163.3, 162.7, 161.1, 160.9, 157.6, 152.5, 148.1, 147.1, 146.9, 131.1, 124.3, 114.7, 114.6, 110.3, 109.9, 108.4, 96.6, 68.3, 66.4, 45.1, 37.1, 31.8, 29.3, 29.2, 26.0, 22.6, 14.1, 12.4. **IR** (neat) ν 3330, 2971, 2920, 2868, 1695, 1598, 1534, 1275, 1131, 1042, 820 cm^{-1}. **HRMS** calcd for $C_{37}H_{47}N_4O_5$ $[M+H]^+$ 627.35410, found 627.3539.

(*E*)-*tert*-Butyl (3-(4-((4-(octyloxy)phenyl)diazenyl)phenoxy)propyl)carbamate (8)

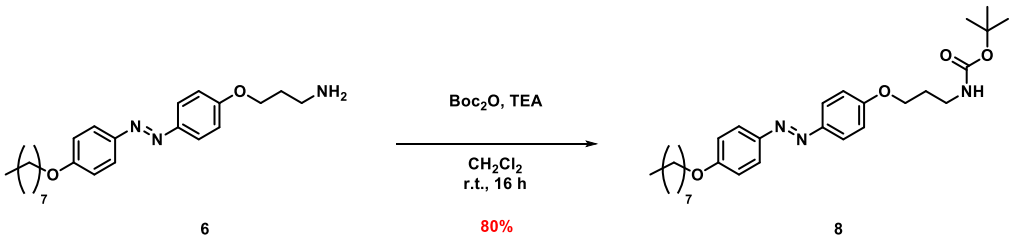

^{1}H NMR (400 MHz, $CDCl_3$): δ 7.88 – 7.80 (m, 4H), 6.99 – 6.94 (m, 4H), 4.74 (s, 1H), 4.07 (t, *J* = 6.0 Hz, 2H), 4.04 – 3.98 (t, 2H), 3.33 (dd, *J* = 12.5, 6.3 Hz, 2H), 2.00 (qui, *J* = 6.1 Hz, 2H), 1.84 – 1.75 (qui, 2H), 1.50 – 1.41 (m, 11H), 1.39 – 1.22 (m, 8H), 0.91 – 0.84 (t, 3H). **^{13}C NMR** (101 MHz, $CDCl_3$): δ 161.2, 160.7, 156.0, 147.1, 146.9, 124.3, 124.3, 114.6, 68.3, 66.0, 37.9, 31.8, 29.5, 29.3, 29.2, 28.4, 26.0, 22.6, 14.1. **IR** (neat) ν 3323, 2922, 2855, 1686, 1599, 1581, 1532, 1496, 1242, 1148, 1025, 841 cm^{-1}. **HRMS** calcd for $C_{28}H_{42}N_3O_4$ $[M+H]^+$ 484.31698, found 484.3170.

(*E*)-*tert*-Butyl methyl(3-(4-((4-(octyloxy)phenyl)diazenyl)phenoxy)propyl)carbamate (9)

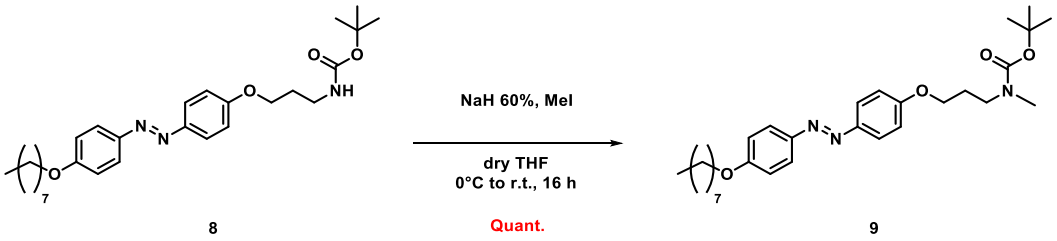

8 9

^{1}H NMR (400 MHz, $CDCl_3$): δ 7.89 – 7.82 (m, 4H), 7.02 – 6.91 (m, 4H), 4.07 – 3.98 (m, 4H), 3.41 (t, *J* = 6.9 Hz, 2H), 2.87 (s, 3H), 2.02 (p, *J* = 6.5 Hz, 2H), 1.79 (p, 2H), 1.52 – 1.38 (m, 11H), 1.38 – 1.24 (m, 8H), 0.86 (t, 3H). **^{13}C NMR** (101 MHz, $CDCl_3$): δ 161.3, 160.9, 155.8, 146.9, 146.7, 124.4, 114.7, 79.4, 68.3, 45.8, 31.8, 29.3, 28.4, 26.0, 22.6, 14.1. **IR** (neat) ν 3323, 2923, 2855, 1682, 1595, 1499, 1248, 1147, 1024, 842 cm^{-1}. **HRMS** calcd for $C_{29}H_{44}N_3O_4$ $[M+H]^+$ 498.33263, found 498.3327.

(*E*)-*N*-Methyl-3-(4-((4-(octyloxy)phenyl)diazenyl)phenoxy)propan-1-amine (10)

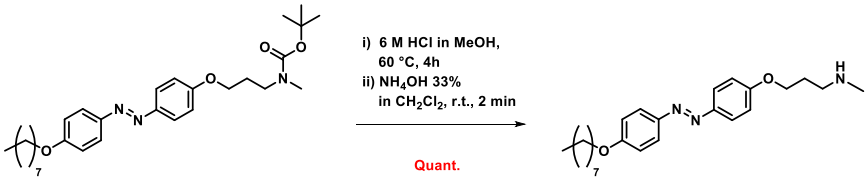

9 10

^{1}H NMR (400 MHz, $CDCl_3$): δ 7.84 (d, *J* = 9.0 Hz, 4H), 6.96 (dd, *J* = 9.0, 3.2 Hz, 4H), 4.09 (t, *J* = 6.2 Hz, 2H), 4.00 (t, *J* = 6.6 Hz, 2H), 2.77 (t, *J* = 7.0 Hz, 2H), 2.44 (s, 3H), 1.98 (p, *J* = 6.5 Hz, 2H), 1.79 (p, *J* = 6.6 Hz, 2H), 1.45 (p, *J* = 6.6 Hz, 3H), 1.39 – 1.25 (m, 9H), 0.86 (t, 3H). **^{13}C NMR** (101 MHz, $CDCl_3$): δ 161.2, 161.0, 147.0, 146.9, 124.3, 114.6, 68.3, 66.6, 48.9, 36.5, 31.8, 29.3, 29.2, 26.0, 22.6, 14.1. **IR** (neat) ν 3300, 2956, 2914, 2849, 1730, 1470, 1179, 1047, 853 cm^{-1}. **HRMS** calcd for $C_{24}H_{36}N_3O_2$ $[M+H]^+$ 398.28020, found 398.2801.

(*E*)-9-(Diethylamino)-2-(3-(methyl(3-(4-((4-(octyloxy)phenyl)diazenyl)phenoxy)propyl)amino)-propoxy)-5*H*-benzo[*a*]phenoxazin-5-one (12)

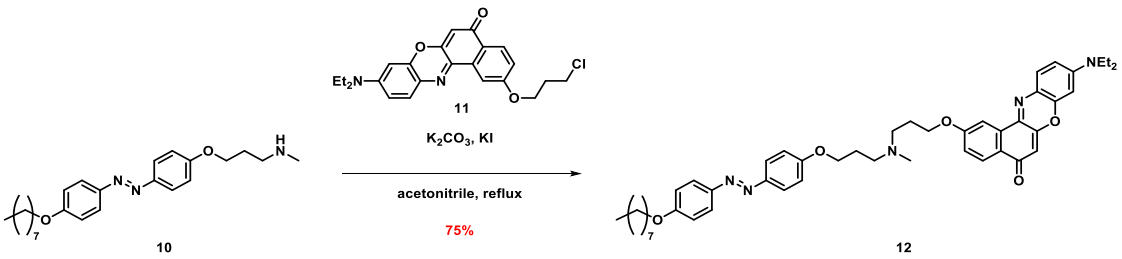

^{1}H NMR (400 MHz, $CDCl_3$): δ 8.15 (d, *J* = 8.7 Hz, 1H), 7.94 (d, *J* = 2.4 Hz, 1H), 7.77 (dd, *J* = 17.2, 8.9 Hz, 4H), 7.51 (d, *J* = 9.0 Hz, 1H), 7.08 (dd, *J* = 8.7, 2.5 Hz, 1H), 6.92 (dd, *J* = 17.0, 9.0 Hz, 4H), 6.58 (dd, *J* = 9.1, 2.6 Hz, 1H), 6.35 (d, *J* = 2.6 Hz, 1H), 6.20 (s, 1H), 4.21 (t, *J* = 5.8 Hz, 2H), 4.08 (t, *J* = 5.8 Hz, 2H), 3.99 (t, *J* = 6.6 Hz, 2H), 3.40 (q, *J* = 7.1 Hz, 4H), 2.92 (dd, *J* = 14.3, 7.2 Hz, 4H), 2.54 (s, 3H), 2.26 – 2.11 (m, 4H), 1.84 – 1.73 (q, 2H), 1.49 – 1.39 (q, 2H), 1.39 – 1.25 (m, 9H), 1.21 (t, *J* = 7.0 Hz, 9H), 0.87 (t, *J* = 6.8 Hz, 3H). **^{13}C NMR** (101 MHz, $CDCl_3$): δ 183.1, 161.2, 160.5, 152.0, 150.7, 147.1, 146.8, 139.7, 134.0, 131.1, 127.7, 125.8, 124.7, 124.3, 124.3, 118.1, 114.6, 114.5, 109.5, 106.5, 105.1, 96.2, 68.3, 65.7, 65.7, 54.0, 45.0, 41.5, 31.8, 29.7, 29.3, 26.0, 25.8, 22.6, 14.1, 12.6. **IR** (neat) ν 3390, 2919, 2850, 1723, 1580, 1497, 1465, 1243, 1147, 1049, 841 cm^{-1}. **HRMS** calcd for $C_{47}H_{58}N_5O_5$ $[M+H]^+$ 772.44325, found 772.4424.

(*E*)-3-((3-((9-(Diethylamino)-5-oxo-5*H*-benzo[*a*]phenoxazin-2-yl)oxy)propyl)(methyl)(3-(4-((4-(octyloxy)phenyl)diazenyl)phenoxy)propyl)ammonio)propane-1-sulfonate (13)

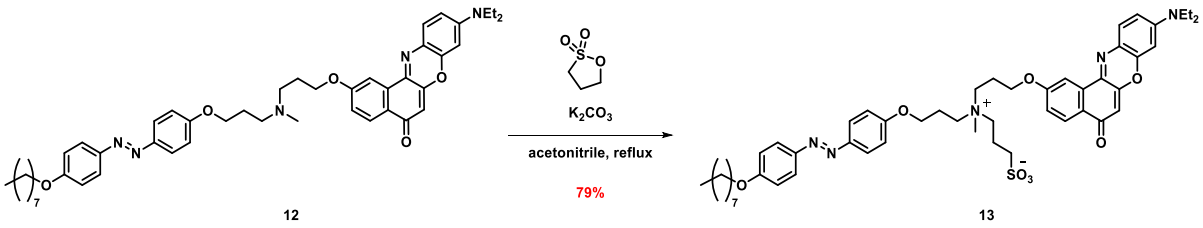

^{1}H NMR (400 MHz, CD_2Cl_2): δ 7.95 (d, *J* = 8.3 Hz, 1H), 7.65 (t, *J* = 8.3 Hz, 4H), 7.58 (s, 1H), 7.22 (d, *J* = 8.7 Hz, 1H), 7.06 (d, *J* = 8.5 Hz, 1H), 6.90 (d, *J* = 8.6 Hz, 2H), 6.80 (d, *J* = 9.1 Hz, 2H), 6.34 (d, *J* = 8.7 Hz, 1H), 6.07 (s, 1H), 5.85 (s, 1H), 5.31 (t, 1H), 4.04 (s, 3H), 3.87 (t, *J* = 6.4 Hz, 2H), 3.77 – 3.49 (m, 5H), 3.26 (d, *J* = 14.8 Hz, 10H), 3.04 – 2.83 (m, 1H), 2.44 (s, 1H), 2.22 (s, 4H), 1.71 (p, *J* = 6.7 Hz, 2H), 1.45 – 1.37 (m, 2H), 1.37 – 1.24 (m, 11H), 1.10 (t, *J* = 7.1 Hz, 6H), 0.87 (t, 3H). **^{13}C NMR** (101 MHz, CD_2Cl_2): δ 182.2, 161.2, 160.6, 160.2, 151.6, 150.6, 147.0, 146.5, 146.3, 138.7, 133.7, 130.8,

129.3, 127.4, 125.5, 124.4, 124.2, 117.7, 114.8, 114.4, 109.5, 106.7, 104.5, 95.7, 68.3, 64.8, 61.3, 58.8, 58.5, 48.8, 47.7, 44.9, 44.6, 31.8, 29.6, 29.4, 29.2, 25.9, 22.6, 22.4, 18.7, 13.8, 12.4. **IR** (neat) ν 3408, 2921, 2851, 1592, 1408, 1181, 1114, 1041, 839 cm^{-1}. **HRMS** calcd for $C_{50}H_{64}N_5O_8{}^{32}S$ $[M+H]^+$ 894.44701, found 894.4461.

2. Synthesis and Photoresponsive properties of amphiphile S1

A coumarin-containing photoswitchable amphiphile was previously synthesized using the route shown in the Scheme below. Coupling of 7-(diethylamino)coumarin-3-carboxylic acid with amine **7** in the presence of 1-ethyl-3-(3-dimethylaminopropyl)carbodiimide (EDC) and 4-dimethylaminopyridine (DMAP) afforded the coumarin-labelled amphiphile **S1** in 24% yield over 6 steps (from nitrophenol **1**).

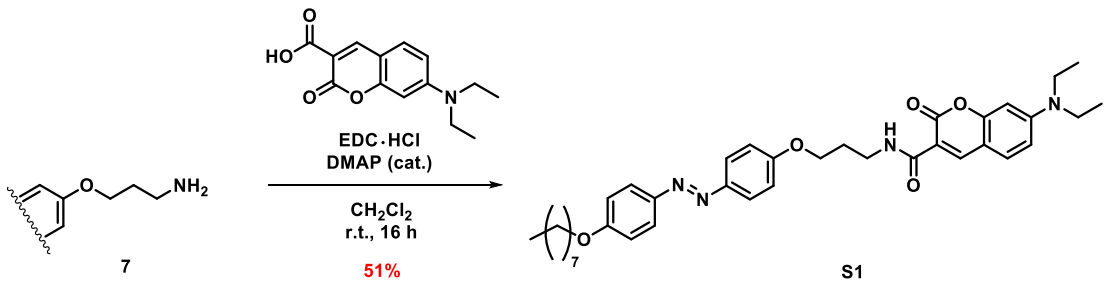

(*E*)-7-(Diethylamino)-*N*-(3-(4-((4-(octyloxy)phenyl)diazenyl)phenoxy)propyl)-2-oxo-2*H*-chromene-3-carboxamide (S1)

To a stirred solution of 7-(diethylamino)coumarin-3-carboxylic acid (18.4 mg, 0.071 mmol, 1.1 eq.) in CH_2Cl_2 (0.6 mL) was added EDC hydrochloride (16 mg, 0.083 mmol, 1.3 eq.) and DMAP (2.0 mg, 0.016 mmol, 0.25 eq.), followed by primary amine **7** (24.6 mg, 0.064 mmol, 1.0 eq.). The resulting suspension was stirred at r.t. for 16 h, after which the solvent was evaporated. Purification of the crude residue by flash column chromatography on silica gel (MeOH/CH_2Cl_2 1:40) afforded the *title compound* as a yellow solid (22.4 mg, 0.032 mmol, 50%).

The photoresponsive properties of azobenzene were retained in the amphiphilic molecule **S1** and the switching between the *E* and *Z* forms could be reversibly driven by illumination with UV and Visible light (**Figure S1**). However, examination of the spectral properties of amphiphile S1 revealed an absorption maximum of 419 nm, meaning that the absorption maximum of the 7-(diethylamino)coumarin moiety overlapped with the absorption of the diazobenzene moiety (**Figure S1b**), resulting in poor emission properties (**Figure S2**). The incompatibility of the coumarin probe with the diazobenzene moiety led us to explore the synthesis of an amphiphile that incorporates Nile red as a fluorescent probe (**13**).

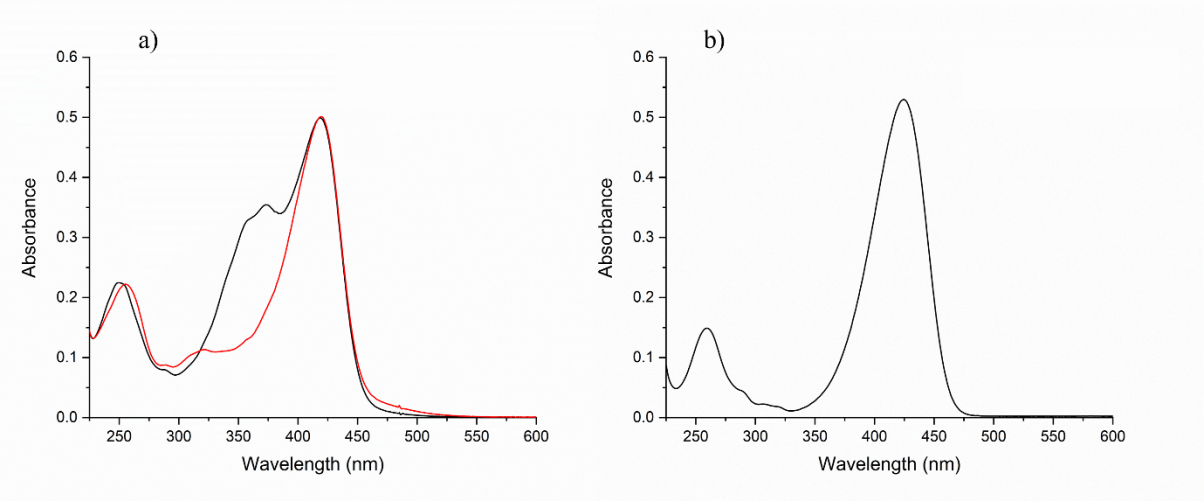

Figure S1. Absorbance spectra showing a) *E* (black line) and *Z* (red line) isomers of amphiphile **S1** (150 µM in methanol). b) 7-(diethylamino)coumarin-3-carboxylic acid (150 µM in methanol).

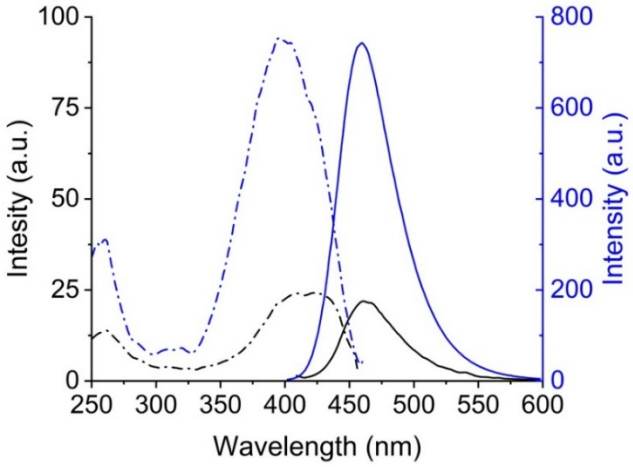

Figure S2. Excitation (dotted lines) and emission (full lines) spectra of [7-(diethylamino)coumarin-3-carboxylic acid] = 15 µM (blue lines) and amphiphile **S1** = 15 µM (black lines) in MeOH. The instrument was set as follows: for the excitation spectrum, λ_{em} 475 nm λ_{em} 250-450 nm; for the emission spectrum, λ_{ex} 375 nm λ_{em} 400-600 nm.

3. Selective photoresponse of amphiphile 13

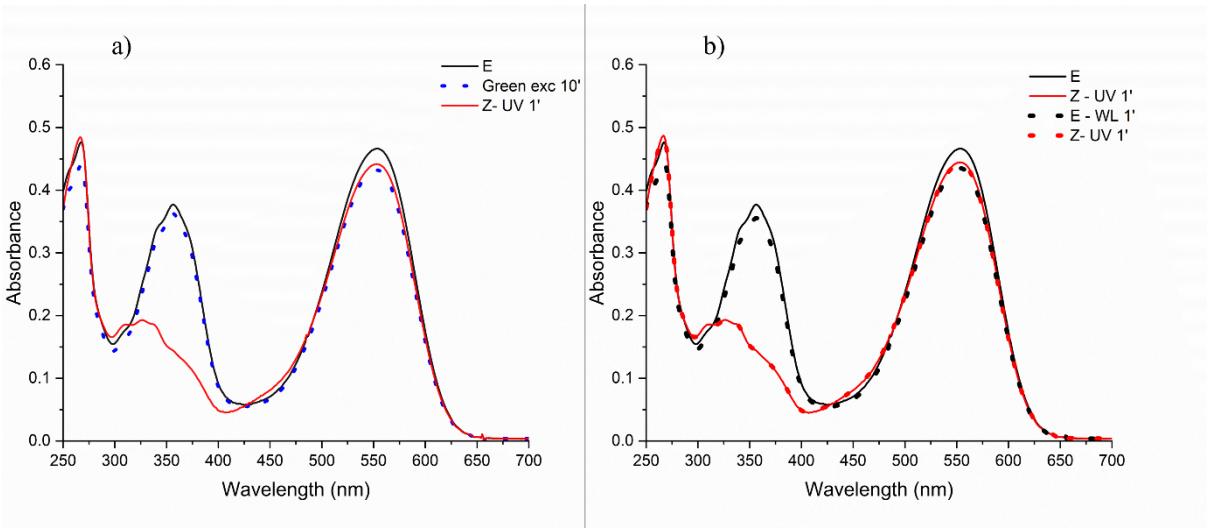

Figure S3. Absorption spectra of amphiphile **13** (15 μM) in ethanol showing: a) the molecule in the *E* isomeric state before (black curve) and after (blue dotted curve) 10 minutes of green light irradiation (510-550 nm). The overlapping of the two curves in the region between 300 and 400 nm shows no *E*-to-*Z* isomerization was induced by the green exciting light. Therefore, Nile red imaging is not interfering with the photoswitch. The red curve represents the *Z* isomer, obtained by subsequently exposing the same sample to UV light (330-385 nm) for 1 minute. Green and UV irradiation were applied directly to the quartz cuvette containing the sample (Hellma Analytics 110-1-40) using a 100 W mercury short-arc lamp (HBO Osram, Wilmington, MA, USA, spectral irradiance ~100 $mW/m^2/nm$) equipped with appropriate band-pass filters. b) Two cycles of *E*-to-*Z* reversible conversion achieved by alternating 1 minute of UV with 1 minute of white light (WL) irradiation. First cycle is indicated by solid lines (black curve, *E* form; red curve *Z* form), while the second cycle is indicated by dotted lines (black curve, reverted *E* form, red curve, *Z* form). Thus, the absorption of Nile red in the blue region does not interfere with the reversibility of the isomerization.

4. Effect of azobenzene photoisomerization on Nile red fluorescence

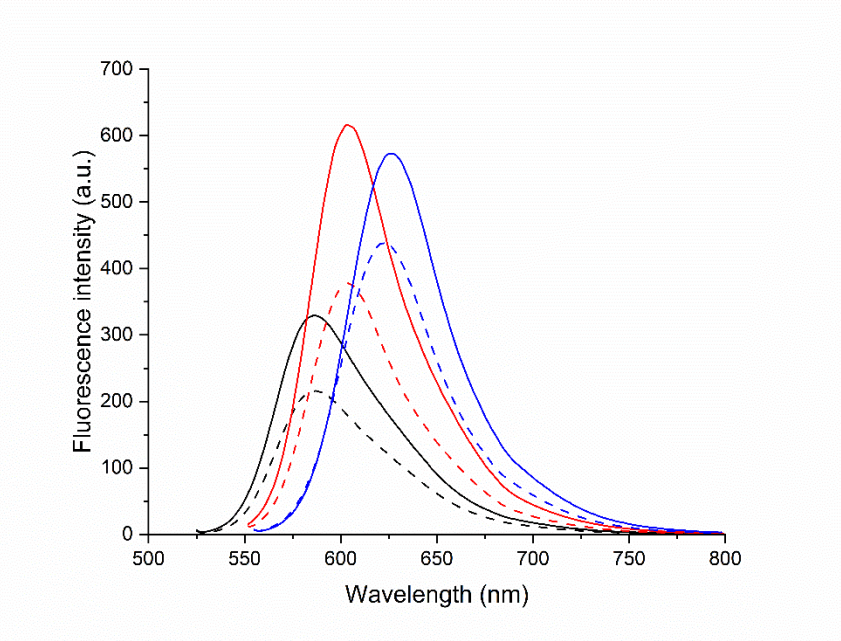

Figure S4 Fluorescence emission spectra of amphiphile **13** (5 μM) in dioxane (black curves), dichloromethane (red curves) or DMSO (blue curves) in the dark (straight lines) and right after 1 minute of UV irradiation (dotted lines). UV irradiation occurred for 1 minute directly on top of the cuvette using an UV portable LED torch (irradiating at λ_{max} = 395 nm) and was switched off immediately before the measurement. In all cases, emission intensity of Nile red moiety in *Z*-isomers decreases by approximately 30% in comparison with the *E*-forms, without any detectable shift in the maximum emission. The intensity drops fully recover almost instantaneously once the UV light is switched off, suggesting a temporal decrease in fluorescence quantum yield due to dynamic quenching associated with the *E*-to-*Z* isomerization of the azobenzene unit. The fluorescence drop during isomerization does not impair the performance of amphiphile **13** as a membrane probe, as illustrated in the confocal micrographs in **Figures 3**, and **S5**.

5. GUV membrane deformation examples

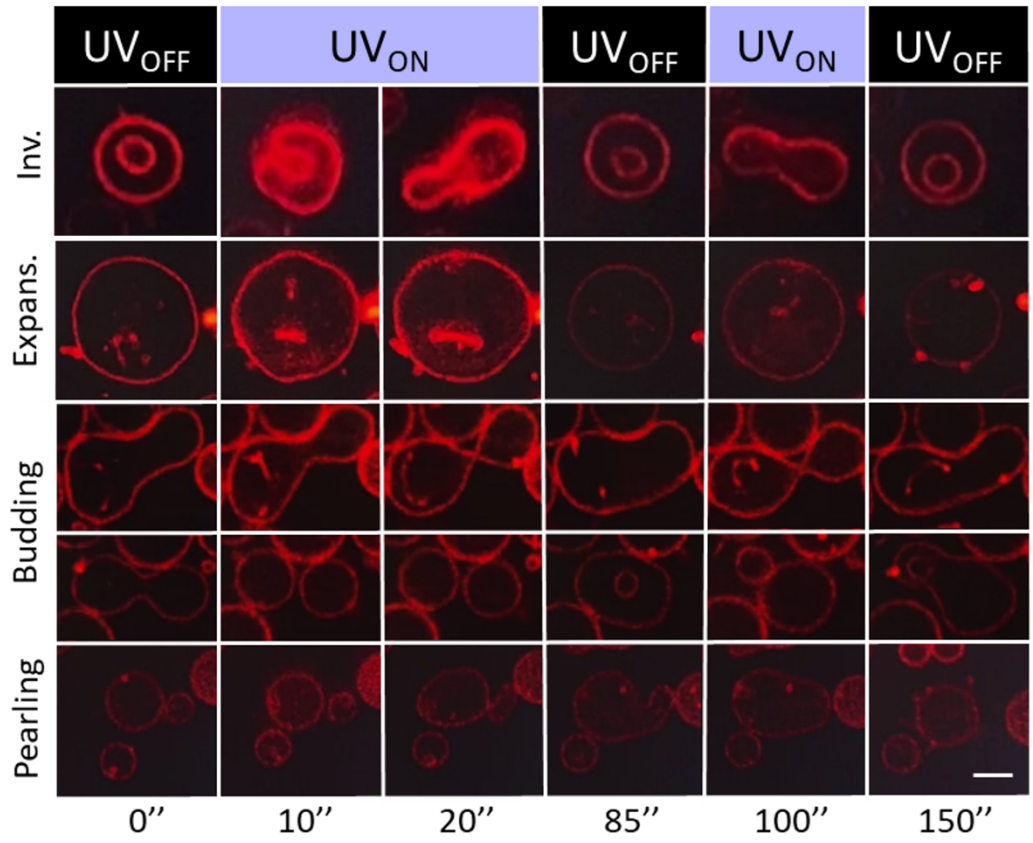

Figure S5. Confocal microscopy images showing UV-induced shape transitions of GUVs containing fluorescent amphiphile **13** (70 μM) in the membrane. The membrane composition is POPC:Cholesterol:**13** in a 1:0.4:0.2 ratio. The five panels illustrate reversible processes such as invagination, expansion, budding and post-fusion pearling. Membrane alterations occur within seconds upon activation and deactivation of the light source. Imaging was performed with λ_{ex} = 515 nm and λ_{em} = 550–700 nm, with *E*-*Z* photoisomerization controlled by the intermittent activation of a 405 nm UV laser. Scale bar: 10 μm.

6. Computational models

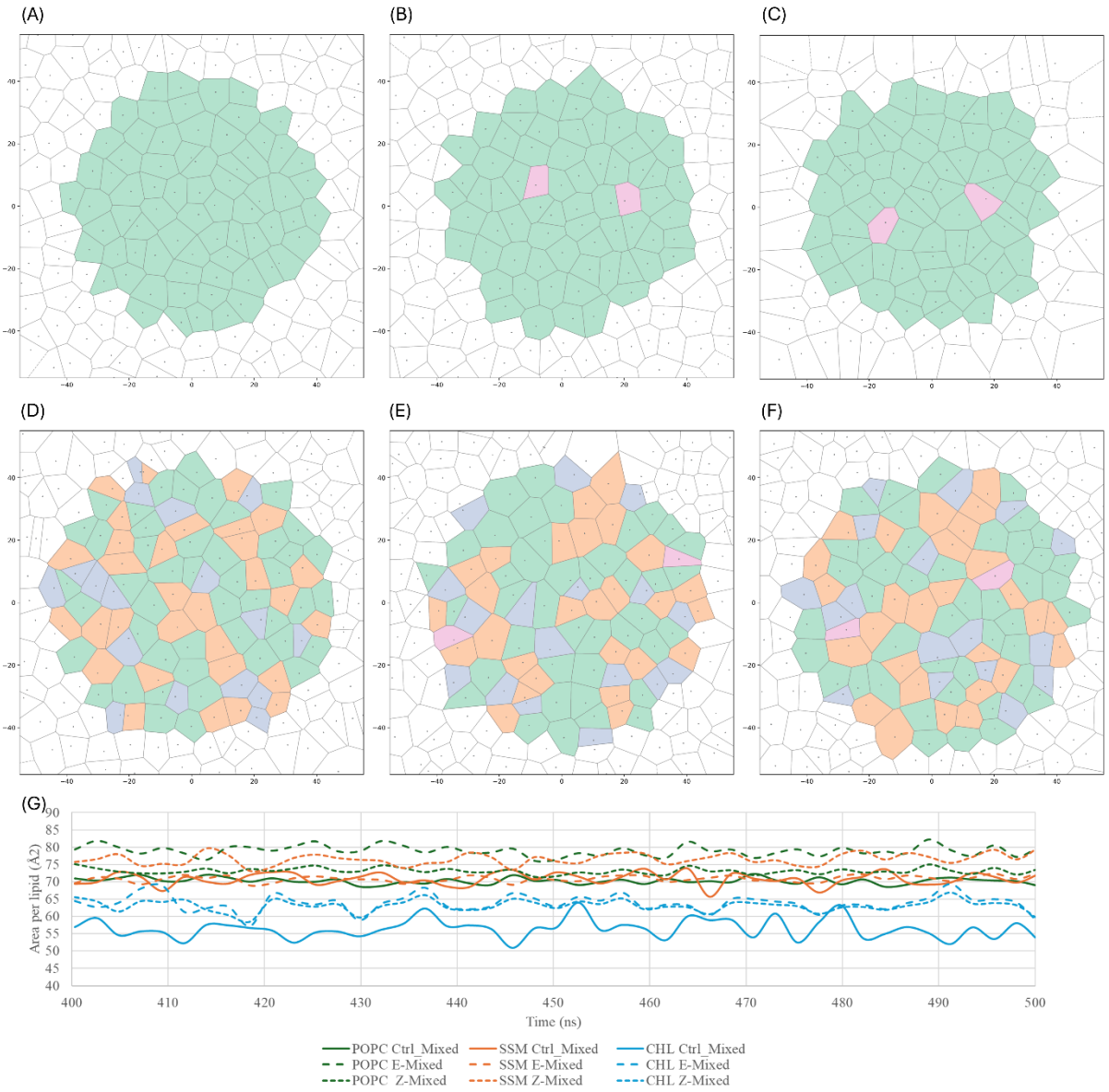

Figure S6. Voronoi tessellation of the upper membrane leaflet of the Ctrl_POPC (A), E-POPC (B), Z-POPC (C), Ctrl_Mix (D), E-Mix (E), Z-Mix (F) after 400 ns of simulation. Polygons are colored according to the type of lipid: POPC (green), SM (orange), cholesterol (light blue), and the photoresponsive amphiphile **13** (pink). (G) Variations in area per lipid (APL) among the models Ctrl_Mixed, E-Mixed and Z-Mixed.

7. Investigation of ROS generation

We investigated whether reactive oxygen species (ROS) are generated upon UV light irradiation of amphiphile **13**, in the presence of the molecular components used in this study. For this purpose, we used the probe dichlorodihydrofluorescein diacetate (H_2DCF-DA), widely applied for detecting intracellular oxidative stress and assess redox analysis in cell-free environments [2-5]. H_2DCF-DA is a chromogenic compound which requires preliminary hydrolysis of the acetate groups to generate 2′,7′-dichlorodihydrofluorescein (H_2DCF), prone to ROS-mediated oxidation. Upon oxidation H_2DCF is converted into the highly fluorescent 2',7'-dichlorofluorescein (DCF, $\lambda_{ex/em}$ = 500/525).

To evaluate the generation ROS in our system, 5 µM H_2DCF-DA was incubated in a quartz cuvette with a solution containing 25 µM amphiphile **13**, 150 µM POPC, 50 mM HEPES (pH 8), and 200 mM glucose:sucrose 1:1, under continuous stirring, at room temperature (20 °C). At pH 8 the probe undergoes chemical hydrolysis to its deacetylated form H_2DCF. As shown in Figure S7a-b, the production of DCF was monitored by measuring fluorescence emission at 525 nm, alternating 3-minute UV irradiation cycles (blue) with dark periods (gray). A delayed and modest ROS generation was observed, starting around 5 minutes after incubation. After 52 minutes, when the oxidation yields 25%, the experiment was terminated by inducing complete oxidation of the probe through the addition of horseradish peroxidase (HRP, 0.1 U/mL) and H_2O_2 (20 mM). No spontaneous autoxidation of the dye was observed in the control sample consisting of 5 µM H_2DCF-DA in 50 mM HEPES pH 8 (data not shown).

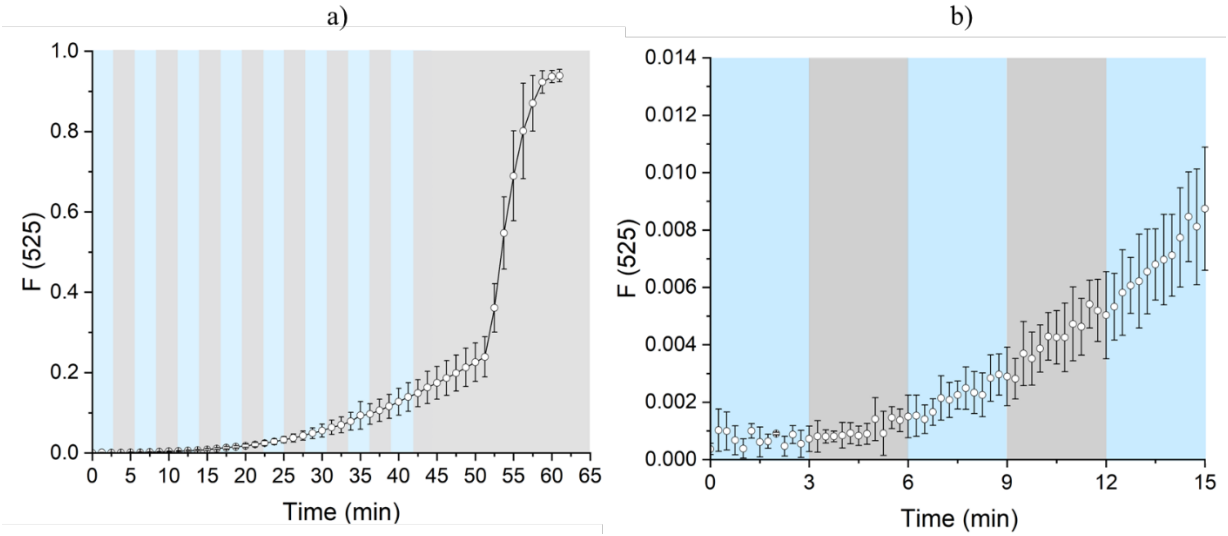

Figure S7. Time-course kinetic of ROS-mediated oxidation of deacetylated H_2DCF-DA to DCF. a) DCF formation was monitored by following its emission at 525 nm. Three-minute UV-illumination cycles and dark periods are alternated during the measurements. At minute 52 HRP and H_2O_2 are added to the cuvette to catalyze complete oxidation of the probe. b) First 15 minutes of curve a). The experiment was performed in triplicates at room temperature (20 °C). Error bars represent standard deviation.

The graphs indicate that ROS generation does not follow light-dependent dynamics and lacks the temporal responsiveness observed in GUV- and LUV-based systems, which display a clear and rapid light-triggered on/off behavior. Therefore, ROS formation cannot be considered the driving factor behind GUV shape transformations or LUV cargo release.

8. NMR characterization data for synthesized compounds

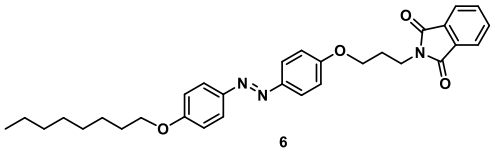

6

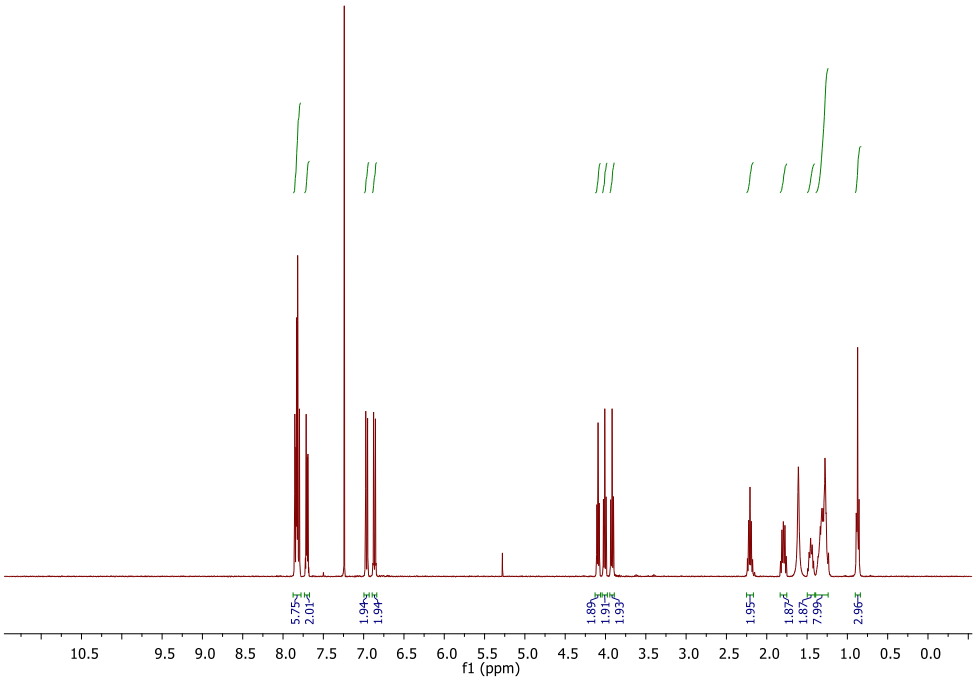

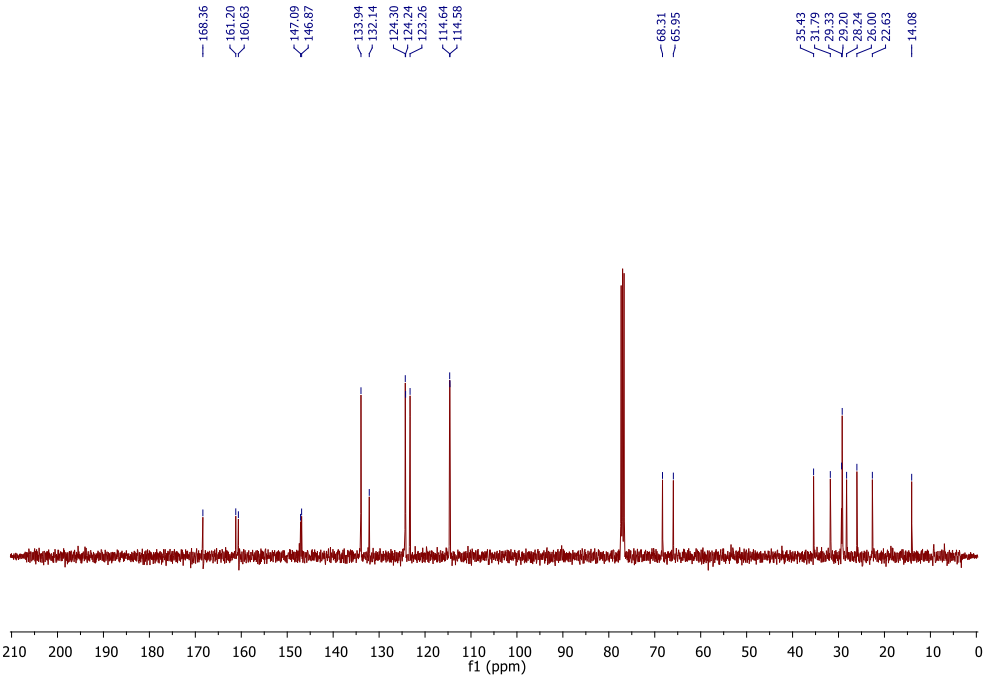

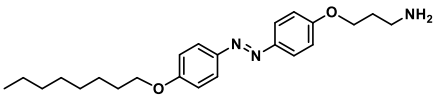
NH2
O
N
N
O

7

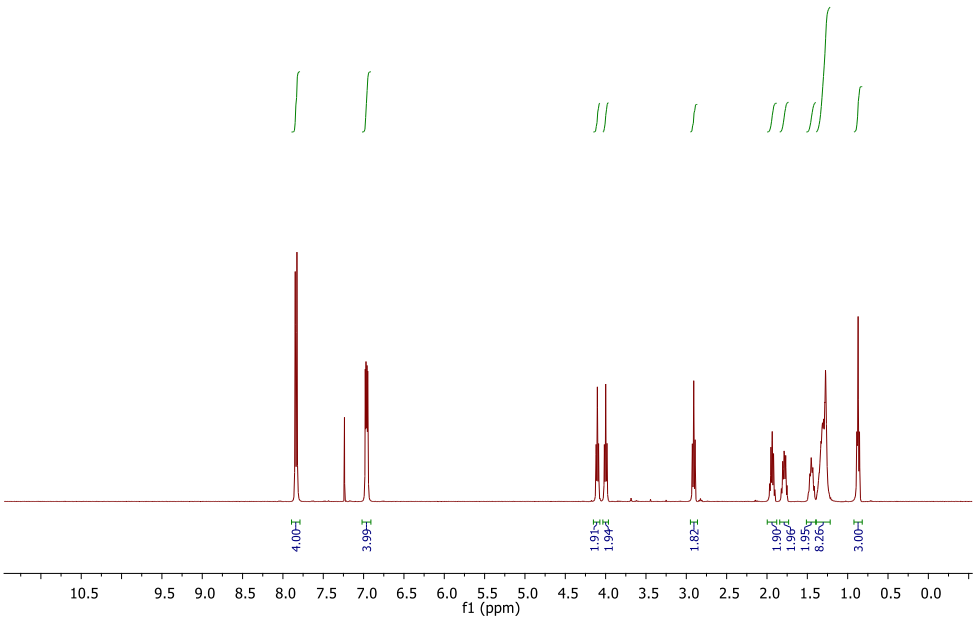
4.00
3.99
1.91
1.94
1.82
1.90
1.96
1.95
8.26
3.00
10.5 9.5 9.0 8.5 8.0 7.5 7.0 6.5 6.0 5.5 5.0 4.5 4.0 3.5 3.0 2.5 2.0 1.5 1.0 0.5 0.0
f1 (ppm)

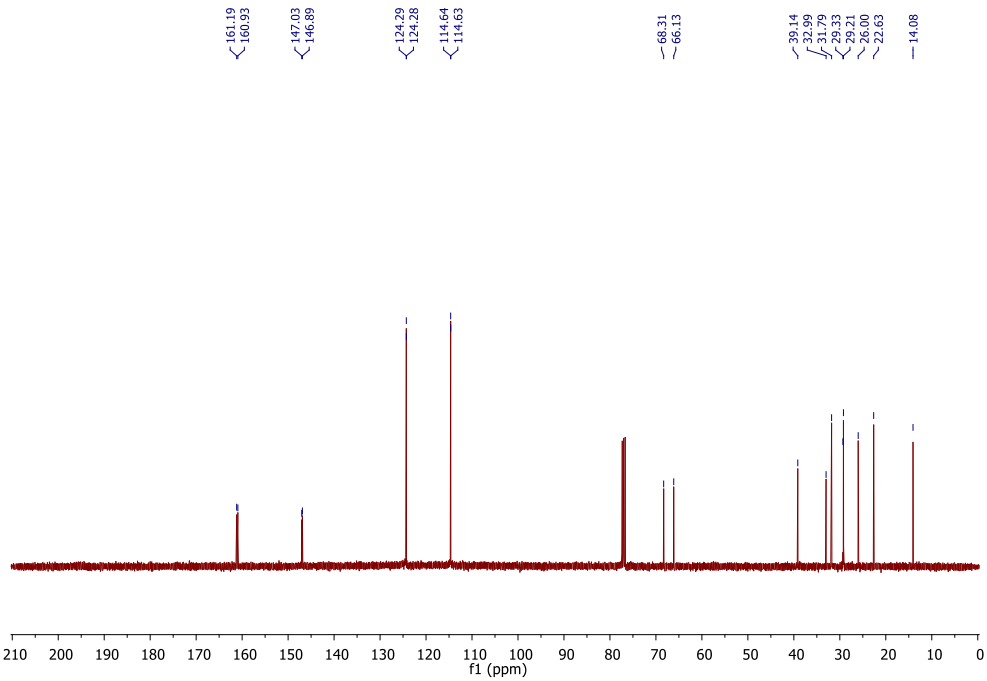
161.19
160.93
147.03
146.89
124.29
124.28
114.64
114.63
68.31
66.13
39.14
32.99
31.79
29.33
29.21
26.00
22.63
14.08
210 200 190 180 170 160 150 140 130 120 110 100 90 80 70 60 50 40 30 20 10 0
f1 (ppm)

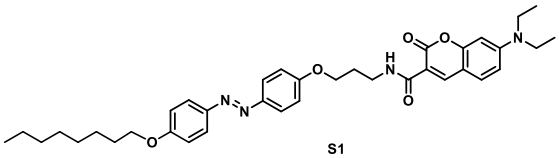

S1

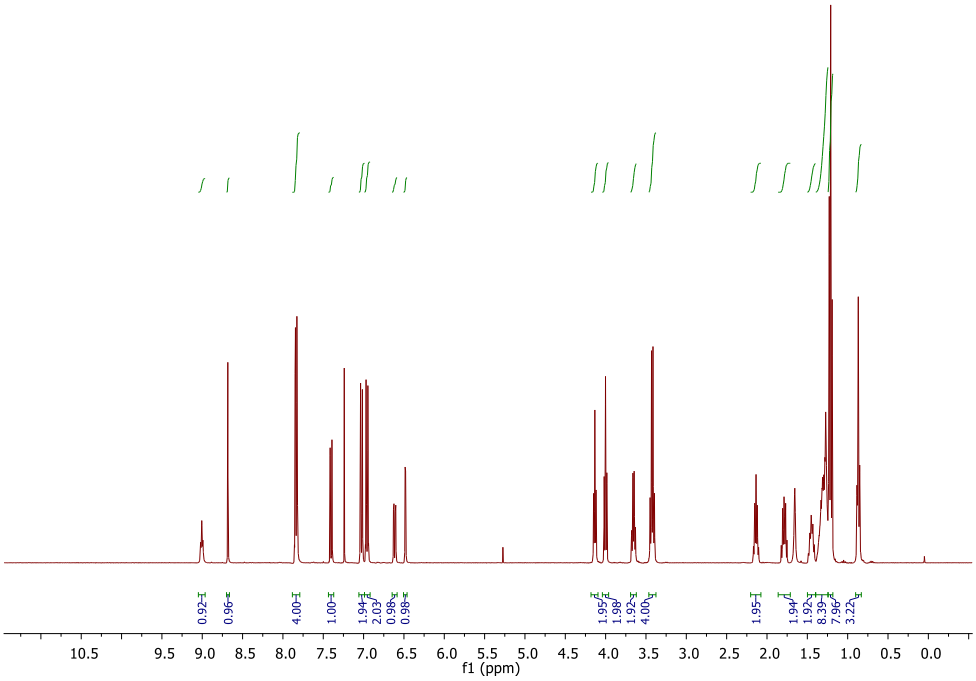
0.92
0.96
4.00
1.00
1.94
2.03
0.98
0.98
1.95
1.98
1.92
4.00
1.95
1.94
1.92
8.39
7.96
3.22
f1 (ppm)

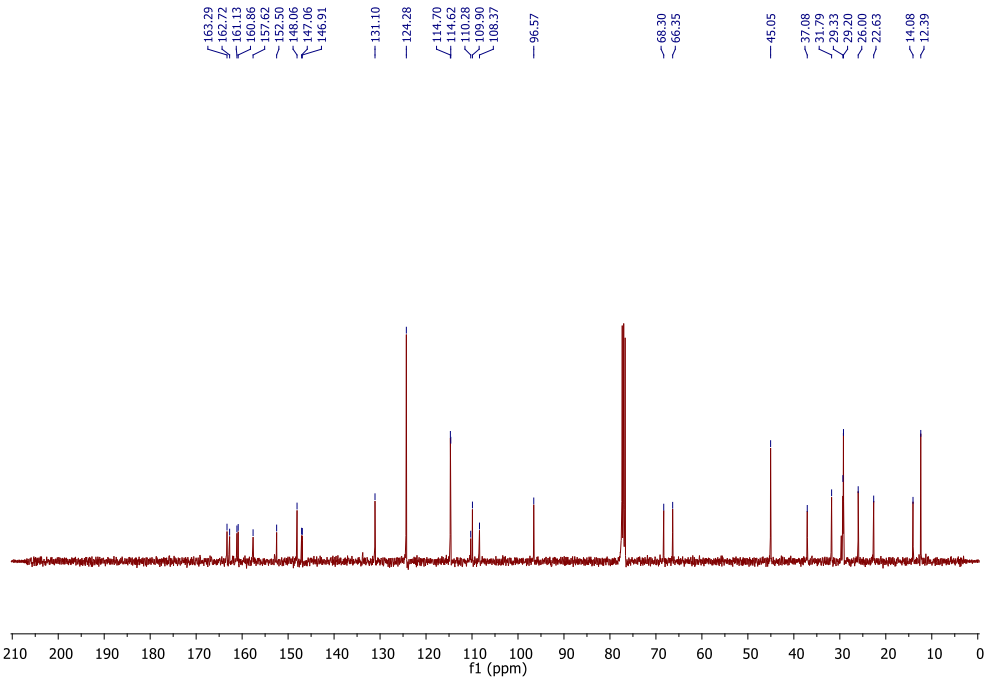
163.29
162.72
161.13
160.86
157.62
152.50
148.06
147.06
146.91
131.10
124.28
114.70
114.62
110.28
109.90
108.37
96.57
68.30
66.35
45.05
37.08
31.79
29.33
29.20
26.00
22.63
14.08
12.39
f1 (ppm)

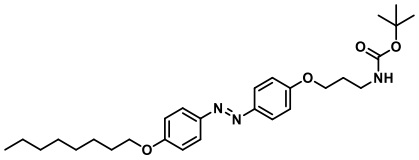

8

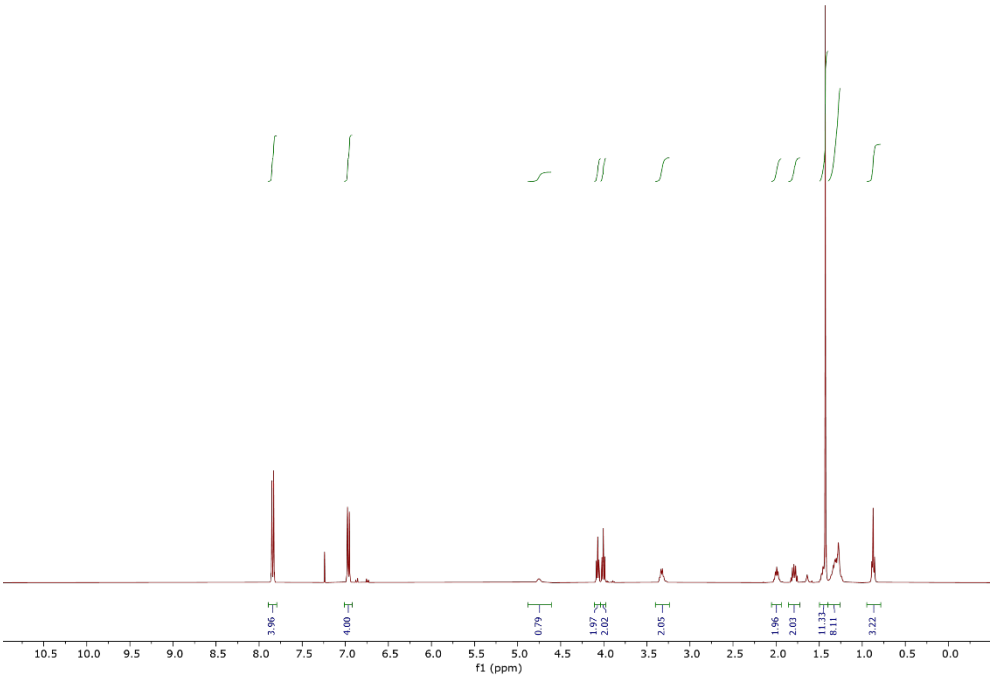
3.96
4.00
0.79
1.97
2.02
2.05
1.96
2.03
11.33
8.11
3.22
f1 (ppm)


161.22
160.68
155.99
147.13
146.87
124.31
124.28
114.64
114.62
68.32
66.02
37.92
31.79
29.53
29.33
29.20
28.39
26.00
22.63
14.08

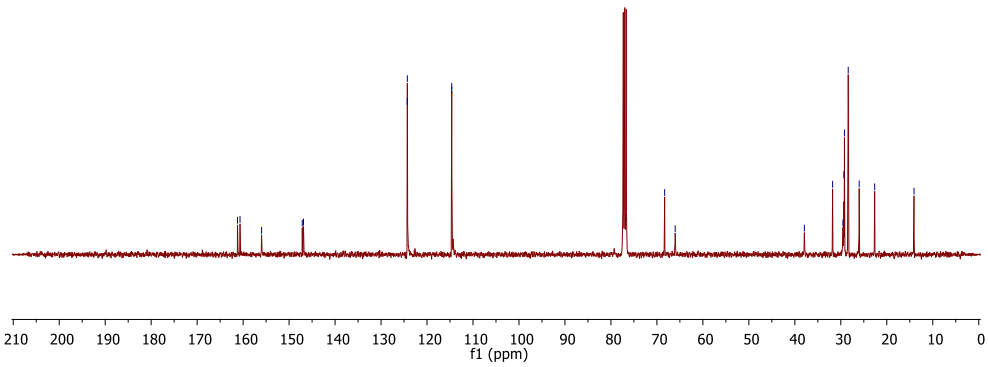
f1 (ppm)

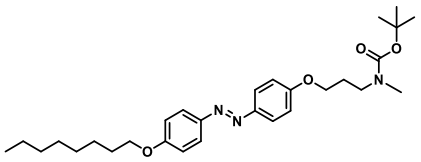

9

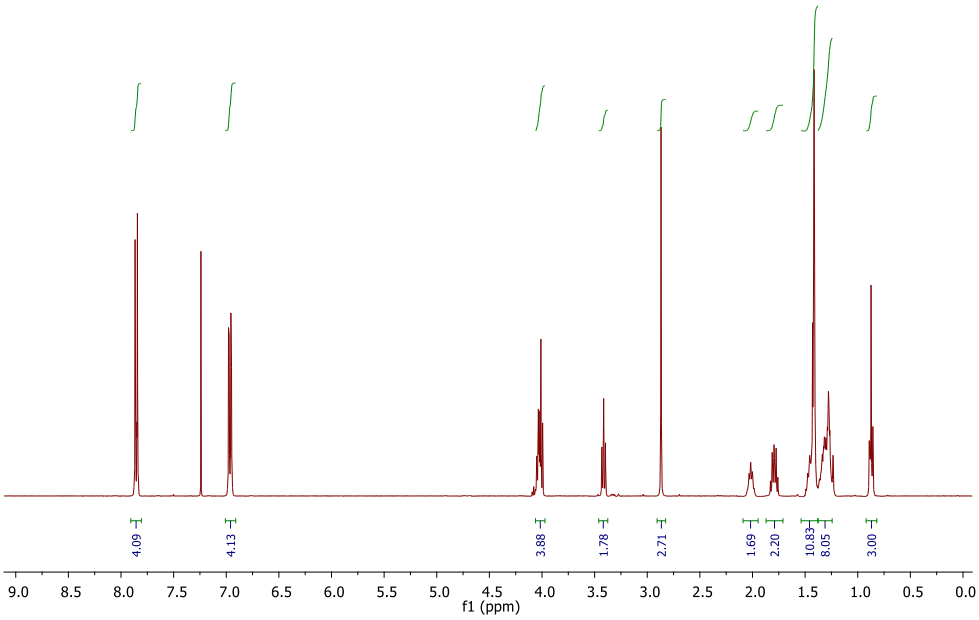
4.09
4.13
3.88
1.78
2.71
1.69
2.20
10.83
8.05
3.00
9.0 8.5 8.0 7.5 7.0 6.5 6.0 5.5 5.0 4.5 4.0 3.5 3.0 2.5 2.0 1.5 1.0 0.5 0.0
f1 (ppm)

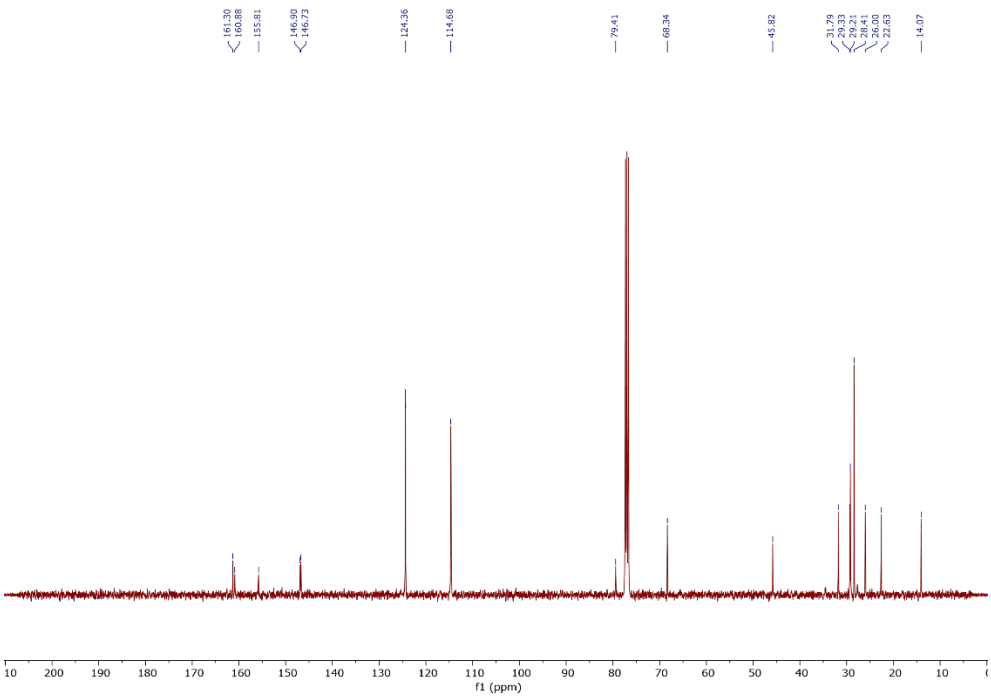
161.30
160.88
155.81
146.90
146.73
124.36
114.68
79.41
68.34
45.82
31.79
29.33
29.21
28.41
26.00
22.63
14.07
10 200 190 180 170 160 150 140 130 120 110 100 90 80 70 60 50 40 30 20 10
f1 (ppm)

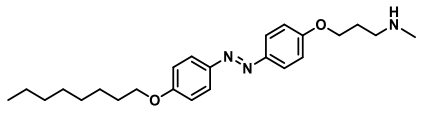

10

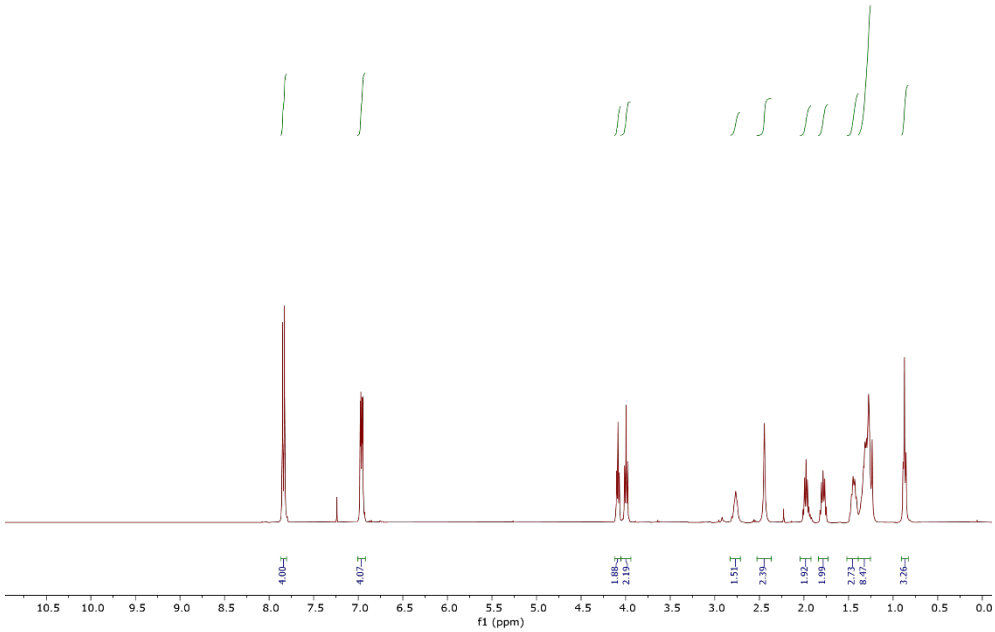
4.00
4.07
1.88
2.19
1.51
2.39
1.92
1.99
2.73
8.47
3.26
f1 (ppm)

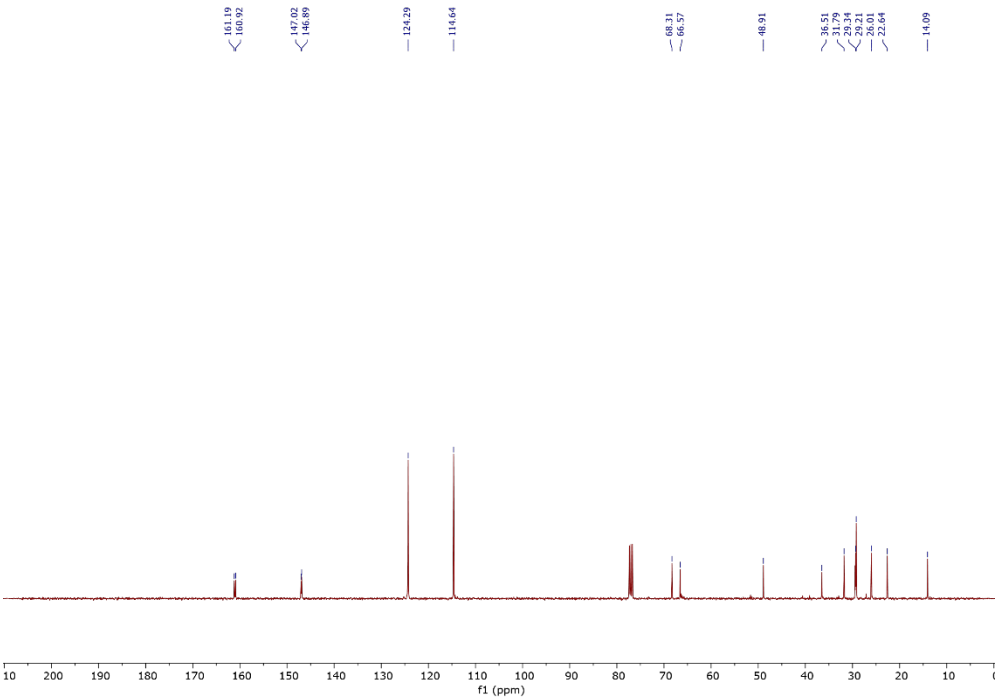
161.19
160.92
147.02
146.89
124.29
114.64
68.31
66.57
48.91
36.51
31.79
29.34
29.21
26.01
22.64
14.09
f1 (ppm)

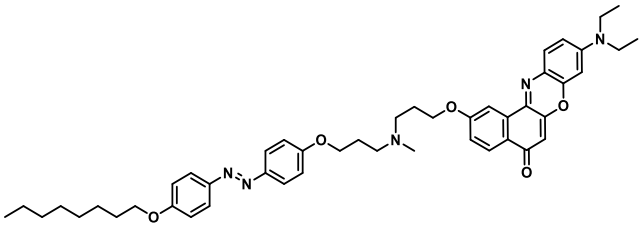

12

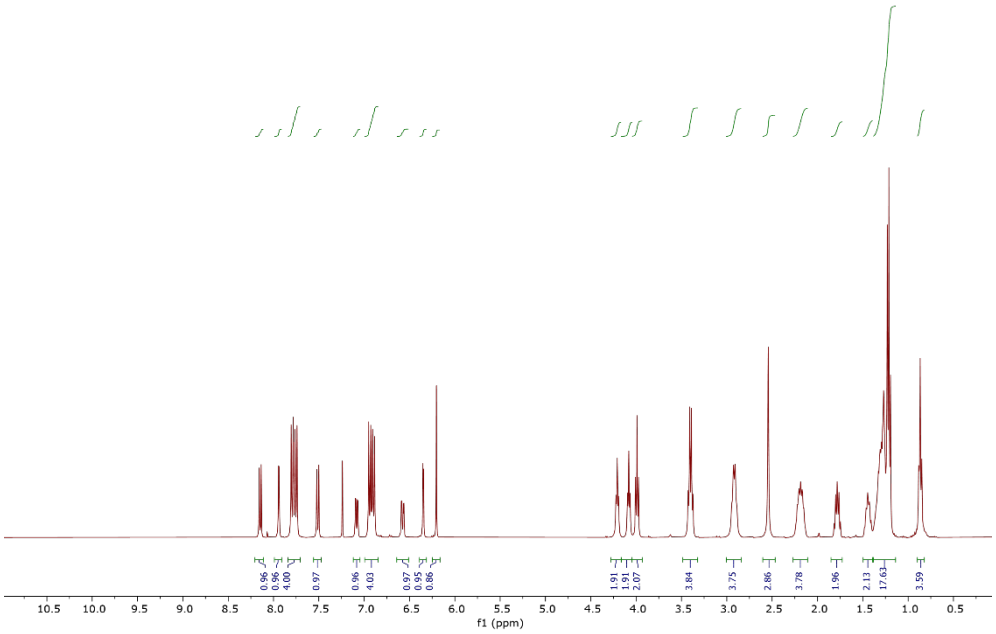
0.96
0.96
4.00
0.97
0.96
4.03
0.97
0.95
0.86
1.91
1.91
2.07
3.84
3.75
2.86
3.78
1.96
2.13
17.63
3.59
10.5 10.0 9.5 9.0 8.5 8.0 7.5 7.0 6.5 6.0 5.5 5.0 4.5 4.0 3.5 3.0 2.5 2.0 1.5 1.0 0.5
f1 (ppm)

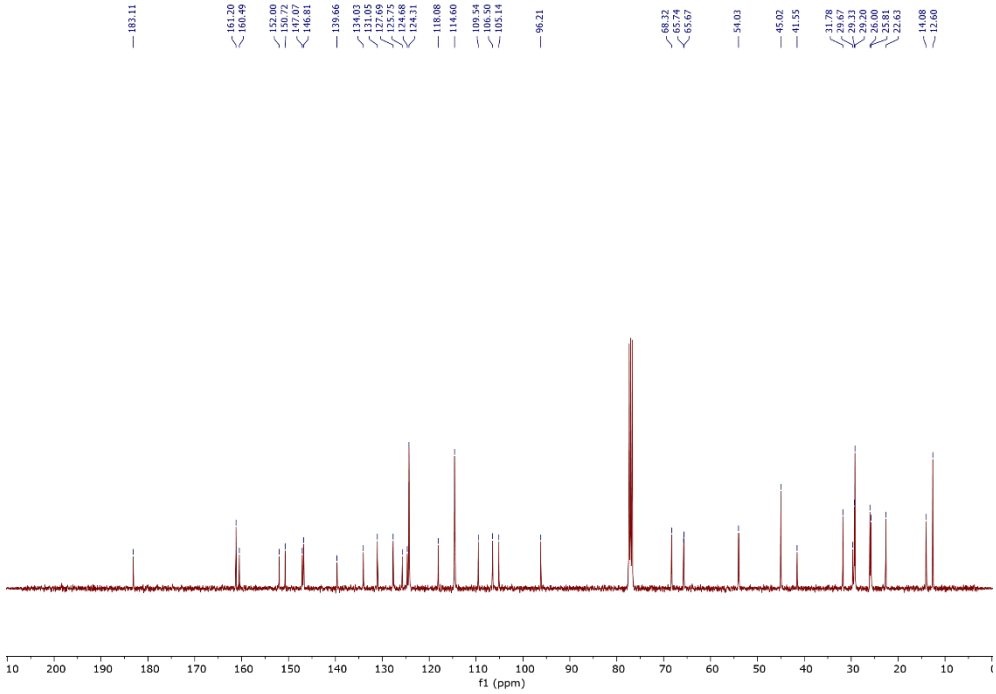
183.11
161.20
160.49
152.00
150.72
147.07
146.81
139.66
134.03
131.05
127.69
125.75
124.68
124.31
118.08
114.60
109.54
106.50
105.14
96.21
68.32
65.74
65.67
54.03
45.02
41.55
31.78
29.67
29.33
29.20
26.00
25.81
22.63
14.08
12.60
10 200 190 180 170 160 150 140 130 120 110 100 90 80 70 60 50 40 30 20 10
f1 (ppm)

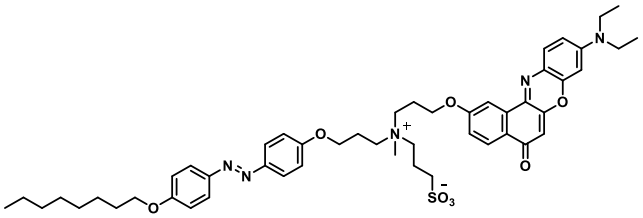

13

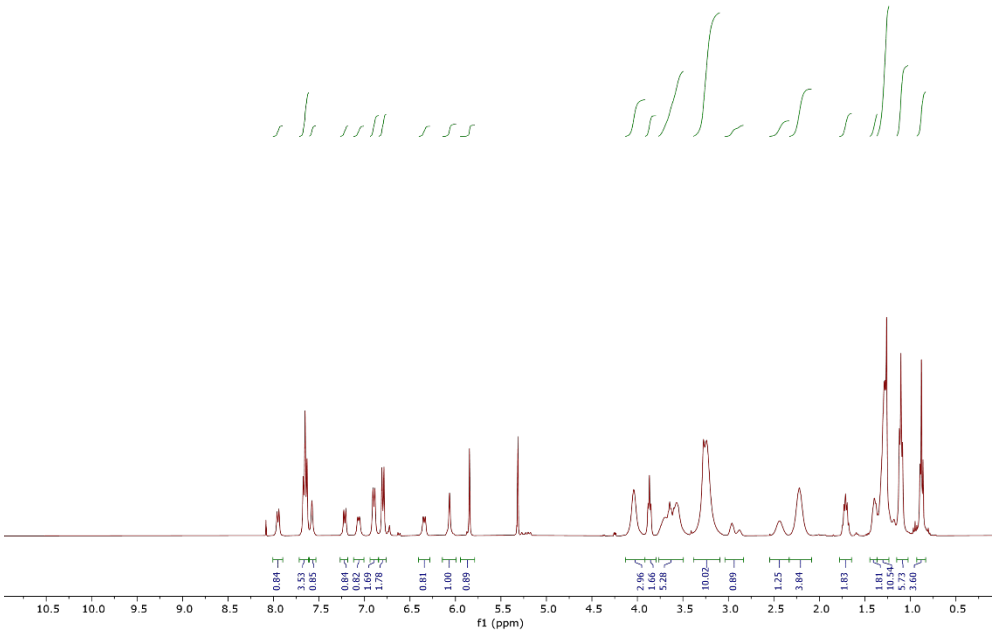
0.84
3.53
0.85
0.84
0.82
1.69
1.78
0.81
1.00
0.89
2.96
1.66
5.28
10.02
0.89
1.25
3.84
1.83
1.81
10.54
5.73
3.60
f1 (ppm)

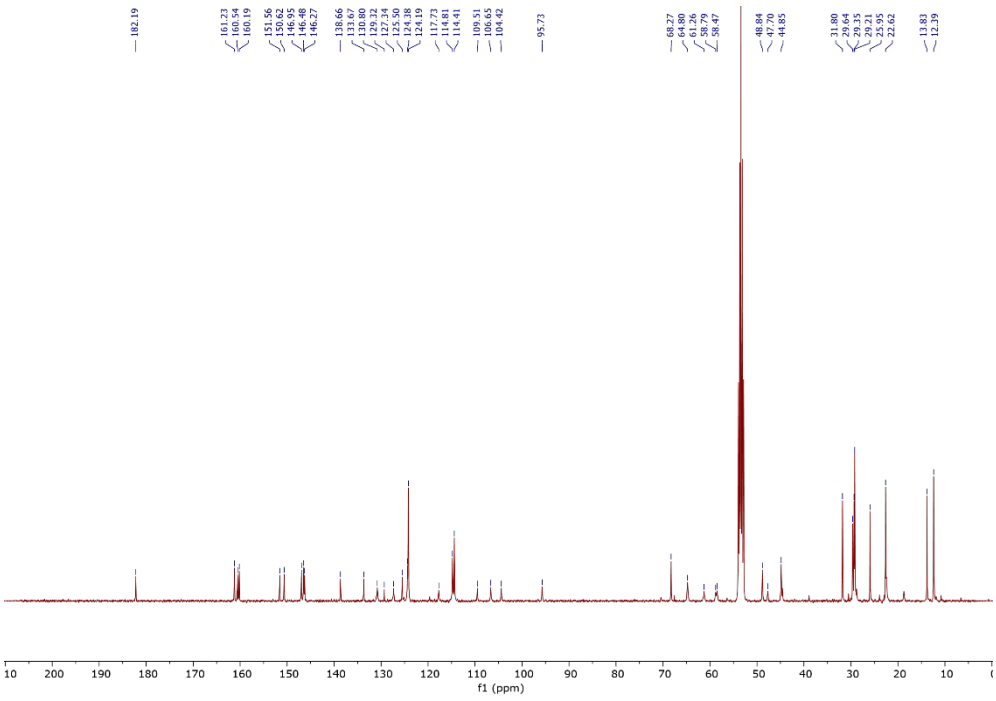
182.19
161.23
160.54
160.19
151.56
150.62
146.95
146.48
146.27
138.66
133.67
130.00
129.32
127.34
125.50
124.38
124.19
117.73
114.81
114.41
109.51
106.65
104.42
95.73
68.27
64.80
61.26
58.79
58.47
48.84
47.70
44.85
31.80
29.64
29.35
29.21
25.95
22.62
13.83
12.39
f1 (ppm)

References

1. E. Wuckert, M. D. Harjung, N. Kapernaum, C. Mueller, W. Frey, A. Baro, F. Giesselmann and S. Laschat, *Photoresponsive ionic liquid crystals based on azobenzene guanidinium salts.* Physical Chemistry Chemical Physics, 2015, 17, 8382-8392.

2. Reiniers M. J., et al., *Preparation and Practical Applications of 2',7'-Dichlorodihydrofluorescein in Redox Assays*. Anal. Chem. 2017. 89, 3853−3857.

3. Eruslanov, E., and Kusmartsev, S., *Identification of ROS using oxidized DCFDA and flow-cytometry*. Methods Mol. Biol., 2010. 594 p. 57-72.

4. Wan, C.P., et al., *An automated micro-fluorometric assay for monitoring oxidative burst activity of phagocytes*. J. Immunol. Methods, 1993. 159 p. 131-138.

5. Setsukinai, K.-I., et al., *Development of novel fluorescence probes that can reliably detect reactive oxygen species and distinguish specific species*. J. Biol. Chem., 2003. 278 p. 3170-5.